Journal Pre-proof

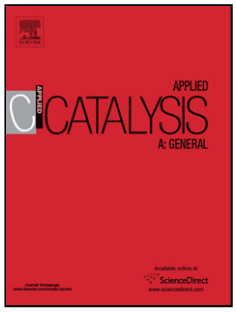

Cellulose Conversion to Biofuel Precursors using Conjugated Ionic Liquid Catalyst: An Experimental and DFT Study

Komal Kumar, Vikas Khatri, Sreedevi Upadhyayula, Hemant K. Kashyap

PII: S0926-860X(20)30544-5

DOI: https://doi.org/10.1016/j.apcata.2020.117951

Reference: APCATA 117951

To appear in: *Applied Catalysis A, General*

Received Date: 24 August 2020

Revised Date: 2 November 2020

Accepted Date: 30 November 2020

Please cite this article as: Kumar K, Khatri V, Upadhyayula S, Kashyap HK, Cellulose Conversion to Biofuel Precursors using Conjugated Ionic Liquid Catalyst: An Experimental and DFT Study, *Applied Catalysis A, General* (2020), doi: https://doi.org/10.1016/j.apcata.2020.117951

Cellulose Conversion to Biofuel Precursors using Conjugated Ionic Liquid Catalyst: An Experimental and DFT Study†

Komal Kumar,[a] Vikas Khatri,[b] Sreedevi Upadhyayula,[a,]*, Hemant K. Kashyap [b,]*

[a] Department of Chemical Engineering, [b] Department of Chemistry, Indian Institute of Technology Delhi, Hauz Khas, New Delhi-110016, India

*Corresponding authors; Tel. No: +91 11 26591083, Fax: +91 11 26591120

E-mails: sreedevi@chemical.iitd.ac.in; hkashyap@chemistry.iitd.ac.in

† Electronic supplementary information (ESI) available.

Graphical abstract

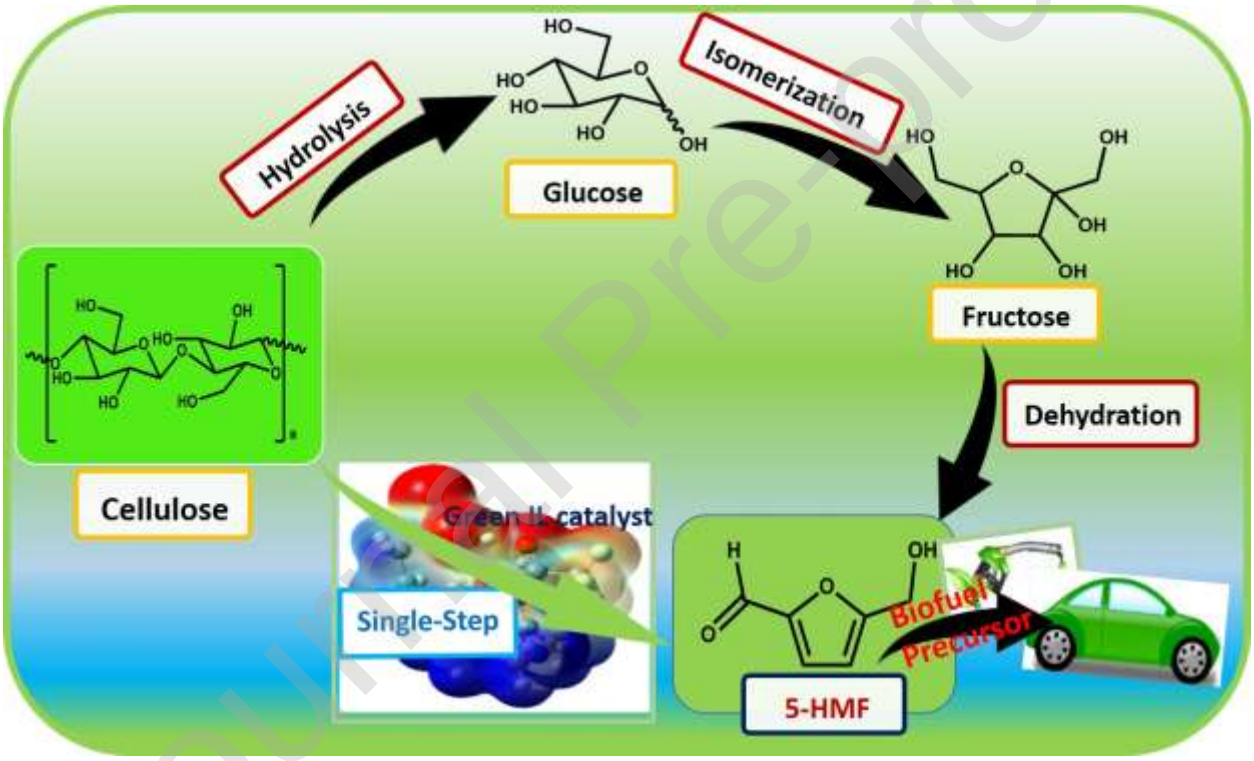

Highlights

- Brønsted acid functionalized 2-Phenylimidazoline based ILs were synthesized.
- Cellulose into biofuel precursors was conducted using IL catalyst.
- Activity of the ILs was compared using both the experimental and DFT results.

- The HOMO and LUMO energies are dominated over the anion and cation of the ILs.
- DFT theory has been used to calculate second order stabilization energy.
- Most energetic interactions between the anions and cations was investigated.

Abstract

In this study, an efficient catalytic system has been developed for the single step conversion of microcrystalline cellulose into 5-hydroxymethyl furfural and levulinic acid using Brønsted acidic ionic liquid (IL) catalysts which have large conjugated structure. The IL catalysts used in this study comprising of different anions ($[CF_3SO_3]^-$, $[HSO_4]^-$, $[CF_3COO]^-$, and $[Cl]^-$) with a common cation 1-butyl sulfonic acid-2-phenylimidazolinium ($[2\text{-PhIm-}SO_3H]^+$), were synthesized in laboratory and characterized. The MCC conversion was carried out in a biphasic reaction medium and yields of 70% for 5-HMF and 23% for LA were achieved at 150 °C and 5 h reaction time. Furthermore, density functional theory (DFT) was performed to identify the key interactions in the stable configurations of the ion-pairs of ILs. The electronic properties and chemical reactivity of the individual ions and ion-pairs of ILs were investigated by performing natural bond orbital (NBO) and second order perturbation theory analyses.

Keywords: Biomass, Ionic liquid, Catalyst, DFT, 5-HMF, Levulinic acid

1. Introduction

The increasing concern about the world's environment and exhaustion of fossil fuel resources [1] has prompted researchers to investigate alternate and clean synthetic routes for the production of fuel and fine chemicals using renewable non-fossil carbon resources [2–4]. 2nd generation biomass is a promising carbon rich sustainable feedstock with wide availability and has been considered as an ideal substitute for fossil feedstock and has enormous potential for production of fuel precursors, fuel additives and other valuable chemicals without threatening the food security [5–7]. Among the promising biomass-derived chemicals, 5-hydroxymethyl furfural (5-HMF) and levulinic acid (LA) have been identified as the most promising chemicals [8,9]. U.S. Department of energy has listed 5-HMF and LA as promising value-added chemicals [10] which can be transformed into a wide range of commodity chemicals, such as 5-hydroxymethylfuroic

acid, furfuryl alcohol, HMF-levulinate [11], 5-furandicarboxlic acid (FDCA), and ethyl levulinate [12,13]. Some of these chemicals can be upgraded into 2, 5-dimethylfuran which can serve as a biofuel component of gasoline, 2,5-furandicarboxylic acid, dihydroxymethylfuran, and 2, 5-diformylfuran [14]. LA can also be catalytically valorized into 2-methyltetrahydrofuran and levulinic acid-esters [15] and the derived esters can be widely used in the pharmaceutical and fuel industries [16]. All these promising uses of 5-HMF and LA have led to an increasing research interest in recent years [17].

The fuel precursors 5-HMF and LA are derived from the dehydration of carbohydrates (monosaccharaides) and are further valorized into fuel, polymers, and also base chemicals [6,18–20]. 5-HMF is also synthesized from the fructose [21,22]. However, high cost of the fructose and its difficult availability prohibits its extensive use for 5-HMF production [20]. Also, the cost of monosaccharaides and ethical issues of using biomass from food crops has decelerated the production of 5-HMF and LA [23,24], which can now be addressed in this route from waste biomass comprising of agricultural residues, forest wastes and also municipal wastes. However, the production of 5-HMF and LA from non-edible and most abundant renewable waste biomass is of great interest. Biomass is composed of three major constituents called cellulose, hemicellulose, and lignin [25,26]. Cellulose, is the more abundant and cheaper biomass constituent which has glucose as a repeating unit linked by β (1→4) glycosidic bond [27] with high crystallinity [28].

Synthesis of the 5-HMF using cellulose includes three steps: (i) formation of glucose from acid hydrolysis of cellulose, (ii) isomerization of the glucose into fructose, (iii) fructose dehydration into 5-HMF and other byproducts [29,30]. Schematic representation of the cellulose conversion into 5-HMF and LA are represented in **Scheme 1**. Different type of the catalyst including mineral acids [31,32] solid acid [33], enzymatic hydrolysis [34], as well as hydrolysis in supercritical water [35] have been used for the conversion of the cellulose into 5-HMF and other value-added chemicals. However, some of the literature reported catalysts gave favorable yields of the desired products on the contrary creates several issues such as high cost of enzymes and their lower thermal stability with low activity [36], reactor corrosion [37], generation of the waste acid sludge, and harsh reaction conditions limiting their scale-up in industry [30,38]. This has raised the need to develop a green, efficient, and environmental benign catalyst–solvent system for the conversion of cellulose into 5-HMF and LA.

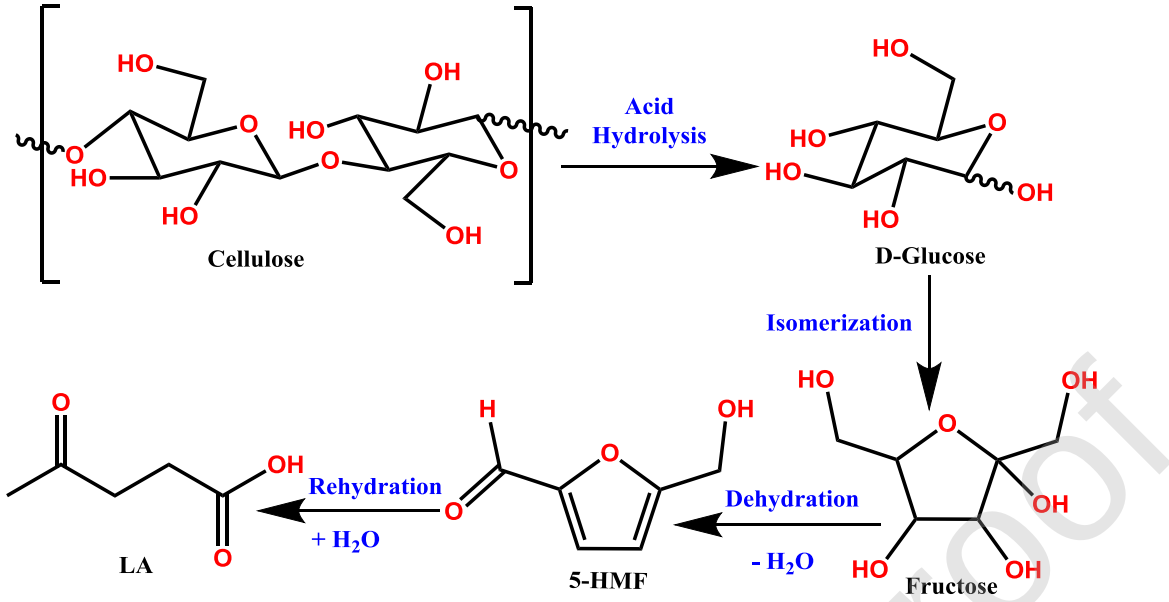

Scheme 1. Schematic representation of acid catalyzed cellulose conversion into 5-HMF and subsequent rehydration into LA.

In this context, ionic liquids (ILs) have received significant attention not only as promising green solvents [39–41], but also as potential catalysts for the dissolution and conversion of the cellulose [42,43]. For instance, R. P. Swatloski et al. reported cellulose conversion using 1-butyl-3-methylimidazolium chloride [BMIM][Cl] ILs [44]. Zhang et al. reported cellulose conversion using ILs [Emim][OAc] and [Amim][Cl] which have lower melting points [45]. Heinze et al. reported cellulose conversion and the obtained results from this study concluded that the pyridinium based [Bpy][Cl] ILs showed better activity for cellulose conversion [46]. Similarly, Sixta et al. claimed that the acid–base conjugated ILs which was prepared by combining the several super-bases (TMG, DBU) with organic acids showed better activity in cellulose conversion [47]. Methylimidazole, 1-vinylimidazole, and triethylamine based ILs was used by Liu and co-workers for cellulose conversion and concluded that the triethylamine based ILs showed impressive results [48]. However, the obtained results from this study indicate that the structure of the ILs have significant effect on the cellulose conversion.

Similarly, the use of the Brønsted acidic ILs for the selective conversion of cellulose into 5-HMF and LA have received extensive interest because of their unique and peculiar properties, such as negligible vapor pressure, adjustable Brønsted acidity [49], low melting temperature [50], high thermal stability, and task specificity [51]. Z. Zhang *et al*. reported 45-60% yield of 5-HMF

using [BMIM][Cl] IL catalyst with $CrCl_3$ [52]. Su *et al*. obtained 55% yield of 5-HMF from cellulose using pairs of the metal chlorides ($CuCl_2$ with $CrCl_2$) with [EMIM][Cl] IL [53]. A good yield of 5-HMF (89%) was achieved in presence of the [EMIM][Cl] with HCl, H_2SO_4 by the addition of the $CrCl_2$. However, the use of the chromium salts are environmentally harmful and are to be avoided and the use of mineral acids produces a lot of waste sludge rendering the overall process environmentally harmful. In presence of the $AlCl_3$, Shaohua *et al.* reported 55% yield of the 5-HMF in the mixed ([BMIM][Cl] with DMSO) solvent [54]. Equipment corrosion is very rampant with the use of $AlCl_3$. On the other hand, the used both the solvent and catalyst in the earlier studies are not hydrophobic in nature which facilitate the 5-HMF formation and selectively required as a reaction medium for the selective conversion of cellulose into5-HMF.

Besides an effective catalyst for 5-HMF synthesis, the solvent also plays a decisive role in high cellulose conversion and high yield of 5-HMF product. Different types of orgainic aprotic solvents such as dimethylformamide (DMF), dimethylacetamide (DMA), dimethyl sulfoxide (DMSO), tetrahydrofuran (THF) and ethyl acetate have been used for 5-HMF and LA synthesis [19]. Protic solvent, water is also used due to its ubiquity and environment-friendliness but the 5-HMF product gets easily rehydrated in aqueous media to LA, formic acid and humins [55,56]. Hence, the use of the high volume ratio of organic phase (hydrophobic solvent) to aqueous phase (hydrophilic solvent) is followed by some researchers in 5-HMF synthesis [57–60]. To our knowledge so far, imidazoline-based ILs which have a hydrophobic benzene ring have not been reported for cellulose conversion to 5-HMF and LA. Hence, the present study is focused on synthesis of 5-HMF and LA from microcrystalline cellulose (MCC) by a single step process using these environmentally benign ILs. The present work choses IL catalyst which has the hydrophobic benzene ring in them and also a hydrophobic solvent to maximize the yield of the 5-HMF from the cellulose conversion.

A series of 2-phenylimidazolinium based Brønsted acidic IL catalyst, having a large conjugation within the five and six membered cyclic rings of its cationic residue $[2\text{-PhIm-}SO_3H]^+$ (1-butyl sulfonic acid-2-phenylimidazolinium), were synthesized in in-house laboratory by choosing task-specific anions for the catalytic conversion of MCC. These IL catalysts are $[2\text{-PhIm-}SO_3H][CF_3SO_3]$, $[2\text{-PhIm-}SO_3H][HSO_4]$, $[2\text{-PhIm-}SO_3H][Cl]$, and $[2\text{-PhIm-}SO_3H][CF_3COO]$ as shown in Fig. 1. The catalytic activity of the synthesized Brønsted acidic IL catalyst were evaluated for the direct one-step conversion of MCC into 5-HMF. The localization/delocalization of the

electron density on the individual ions and ion-pairs of the IL catalysts generated by calculating the electrostatic surface potential (ESP) was assessed. The HOMO-LUMO energies of the orbitals of the IL catalyst, bond dissociation energy, and second order stabilization energy ($E^{(2)}$) of the synthesized catalyst were calculated using DFT. The novelty of this work lies in explaining the use of Brønsted acidic IL catalyst, in an one-pot conversion of MCC to 5-HMF and LA and further explain the catalyst behavior by theoretical DFT calculations. Further, this study also explores the characteristic structural and electronic properties of the ions and ion-pair complexes pertaining to the IL catalysts by preforming quantum chemical calculations using density functional theory (DFT).

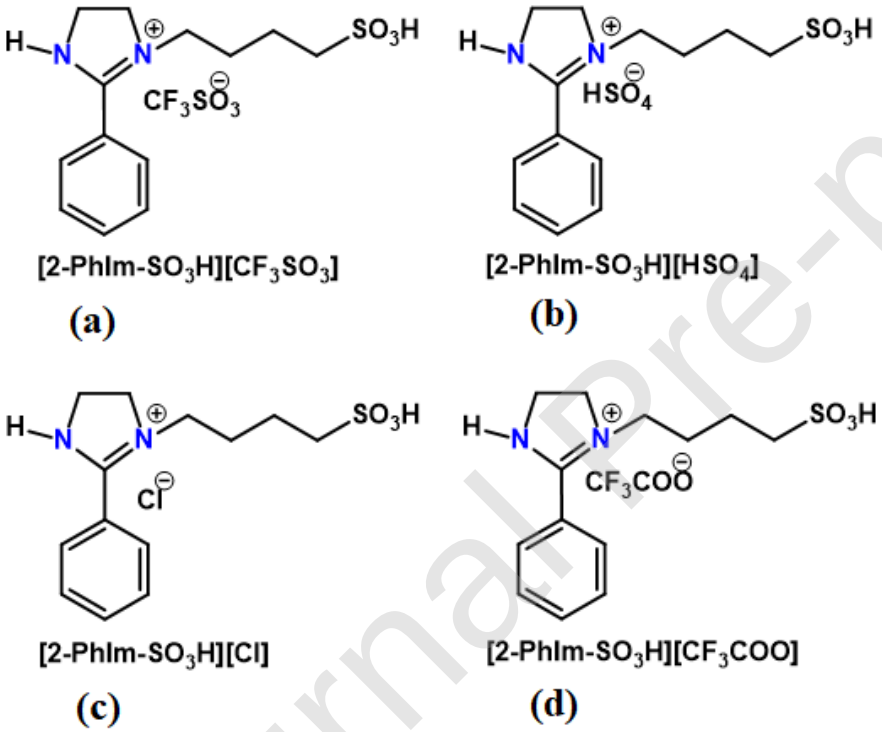

Fig. 1. Structures of (a) [2-PhIm-SO_3H][CF_3SO_3], (b) [2-PhIm-SO_3H][HSO_4], (c) [2-PhIm-SO_3H][Cl], and (d) [2-PhIm-SO_3H][CF_3COO] IL catalysts.

2 Experimental section

2.1 Materials and Methods

Glucose, fructose (99%), 5-HMF (98%), formic acid (FA) (99%), and LA (99%) were purchased from Fisher Scientific, India. 1,6-Anhydro-β-D-glucose (99%), 2-phenylimidazoline, and H_2SO_4 (98%) were purchased from TCI chemicals. 1, 4-butanesultone (99%) were purchased from Alfa

Aesar, China. CF_3COOH and CF_3SO_3H were purchased from Spectrochem India. Diethyl ether, ethyl acetate, and HCl were purchased from Merck, India.

2.2 Synthesis of the Brønsted acidic IL catalysts with different anions

Synthesis of the Brønsted acidic IL catalysts was done following a typical procedure reported in literature [61]. Typically, equimolar amount of 2-phenylimidazoline (1.462 g, 0.01 mol) and 1,4 butane sultone (1.362 g, 0.01 mol) were dissolved in chloroform and this mixture was stirred at 40 °C for 72 h. After the completion of the reaction, the solvent was evaporated under reduced pressure and the zwitterion, thus formed, was washed three times with dichloromethane (DCM) to remove the unreacted materials and dried in vacuum at 50 °C for 24 h to get a yellowish coloured solid. The Brønsted acidic IL catalyst was synthesized by neutralization of the zwitterion by adding a stoichiometric amount of CF_3SO_3H, H_2SO_4, CF_3COOH, and HCl acid to get the corresponding anionic IL after stirring at room temperature for 24 h. The resultant Brønsted acidic IL catalyst was washed with diethyl ether repeatedly and characterized using NMR, mass, and FT-IR spectroscopic techniques as represented in the ESI (Fig. S1-S9).

2.3 Computational details

All the quantum chemistry calculations were performed using density functional theory with B3LYP exchange-correlation functional [62,63]. The optimization of the all the laboratory synthesized Brønsted acidic IL catalysts was performed in gas phase using 6-311++G (d, p) basis set [64] with Gaussian 09 program. The optimized minimum energy configuration of each ion or ion-pair complex was confirmed by frequency calculation in which no imaginary frequency was observed. From the DFT optimized structures, the values of interaction and bond dissociation energies of the Brønsted acidic IL catalysts were calculated and the acidity of the ILs were validated against the experimental data. From the DFT optimized structures, the electrostatic potential (ESP) surfaces on the individual ions and ion-pairs were generated using GaussView 5.0 program [65]. From the DFT optimized structures, the natural bond orbital (NBO) analysis[66] were performed in order to study the intermolecular and intramolecular interactions within the ILs [67]. From the NBO analysis, the interaction of the cation and anion in IL ion-pairs was characterized in terms to identify the most favorable electronic transitions within the ion-pairs of IL catalyst by calculated the second order stabilization energy ($E^{(2)}$) value [68]. The interaction energy (E_{int}) of the ion-pair of an IL catalyst was calculated using the equation,

$$E_{int} = E_{IL} - (E_{cation} + E_{anion}) \qquad (1)$$

where E_{cation}, E_{anion} and E_{IL} are the energies of the isolated cation, anion and ion-pair complex of the IL, respectively. The bond dissociation energy (E_{diss}) for an IL was calculated using the equation,

$$E_{diss} = E_{IL} - (E_{CB} + E_{H^+}), \quad (2)$$

where E_{CB} and E_{H^+} are the energies of the conjugate base and H^+ ion, respectively.

2.4 Acidity measurement of the synthesized IL catalysts

The acidity of the synthesized Brønsted acidic IL catalysts having different anions were determined by previously reported method by calculating the Hammett function [69,70]. 25 mM concentration of the IL catalysts and required molar amount of the 4-nitroaniline were dissolved in water and magnetically stirred for required time. After the mixing of the IL with 4-nitroaniline, spectral scanning was processed from 300 nm to 550 nm by UV–Vis, using double beam Dynamica Spectrophotometer (Model: Halo DB-20) and the absorption was compared to the maximum absorption wavelength (at 380-381 nm) as shown in the Fig. 2(a). The acidity of the synthesized catalysts was calculated by following the Hammett equation:

$$H_0 = pK\,(I)_{aq} + \log(\frac{[I]}{[IH^+]}), \quad (3)$$

where [I] represents the molar concentration of unprotonated 4-nitroaniline and [IH^+] is molar concentration of protonated forms of the 4-nitroaniline in water, and $p\mathrm{K}(I)_{aq}$ is the pKa value of the 4-nitroaniline. The values of Hammett acidity function (H_0) for the IL catalysts investigated are provided in Table 1.

2.5 Characterization of the synthesized Brønsted acidic IL catalysts using experimental and theoretical FT-IR spectroscopy

Experimental FT-IR measurements of the laboratory synthesized ILs were performed using Nicolet-6700 spectrometer in the range of 400-4000 cm^{-1}. The theoretical FT-IR spectra of the ILs were generated by performing the DFT calculation and compared with the experimentally obtained FT-IR spectra as shown in the Fig. 2(b).

2.6 Typical procedure used for the hydrolysis of biomass into 5-HMF and LA using an IL acid catalyst

Cellulose has β (1→4) glycosidic bond within the cellulose structure, which provides rigidity and crystallinity to cellulose, and is insoluble in conventional solvents such as water. Typically, this microcrystalline cellulose (MCC) was initially dried for 24 h at 100 °C to remove moisture, after which, it is catalytically converted in a 25 mL autoclave with 4-methyl-2-pentanone (MIBK) and

water as biphasic solvent using lab synthesized IL catalyst at the desired reaction temperature using a silicon oil bath whose temperature is set and monitored at ± 2 °C under autogenous pressure and continuous stirring using Tarson Magnetic stirrer until reaction reached completion. After the completion of the reaction, heating was terminated by immediately quenching the batch reactor in a cold ice bath. After the reaction, three layers organic, aqueous, and solid were clearly identified and the solid residue from the reaction mixture was separated by centrifugation and dried at 50-100 °C for 8-10 h. The conversion of cellulose was then calculated following earlier reported procedure [29,71]. Further, MIBK from the reaction mixture was evaporated using rotary vacuum evaporator and diluted with water and the product from the aqueous phase was extracted using ethyl acetate which was again evaporated using rotary vacuum evaporator and analyzed to assess the quantitative yields of the products.

2.7 Product yield determination using HPLC

Quantitative analysis of the products yield was done using Agilent high pressure liquid chromatography (HPLC, Agilent Technologies) and HPX-87H column (300∗7.7 MM) with 0.5 mM H_2SO_4 as a mobile phase. During the sample analysis, the flow rate and column temperature were kept constant as 0.5 mL/min and 65 °C, respectively, by maintaining the RID detector (refractive index detector) temperature 35 °C. The injection volume of the sample was 10 µL and detected with RID detector. The samples were filtered using 0.22 µm syringe filter prior to the HPLC analysis. Yield of the products was calculated based on the standard curve obtained using external standard of the products.

3. Results and discussion

3.1 Characterization of the synthesized Brønsted acidic IL catalysts

3.1.1 Experimental and theoretical FT-IR spectra of the synthesized IL catalysts

A comparison of the experimentally measured FT-IR spectra of the four IL catalysts is shown in Fig. S9 of ESI. Characterization of the lab synthesized IL catalyst ([2-PhIm-SO_3H][CF_3SO_3]) was carried out using experimentally measured and theoretically calculated FT-IR spectra and are compared as shown in Fig. 2(b). Theoretical FT-IR spectrum of the IL catalyst is found to be correlated with the experiment by the factor of 0.94 [72]. The experimental FT-IR spectrum of the catalyst displayed a broad peak at 3300-3600 cm^{-1} which represents the O-H stretching of the SO_3H functional group. In the experimental and theoretical FT-IR spectra, the peaks in the range of 2810-3020 cm^{-1} may be attributed to the C-H stretching vibrations of the aliphatic butyl chain

which is attached with the 2-phenylimidazoline. Appearance of a strong peak in the range of 1528-1690 cm^{-1} attributed to the carbon-carbon stretching in the five membered ring and have good agreement between theoretical and experimental data [73]. A sharp peak at 1115-1180 cm^{-1} is associated with the C-N bond which is present within the five membered ring and found similar in both experimental and theoretical results. Peak in the range 1030-1037 cm^{-1} is associated with the S=O bond in SO_3H [74]. Thus, the obtained experimental and theoretical FT-IR spectra are in good agreement for the laboratory synthesized IL catalysts.

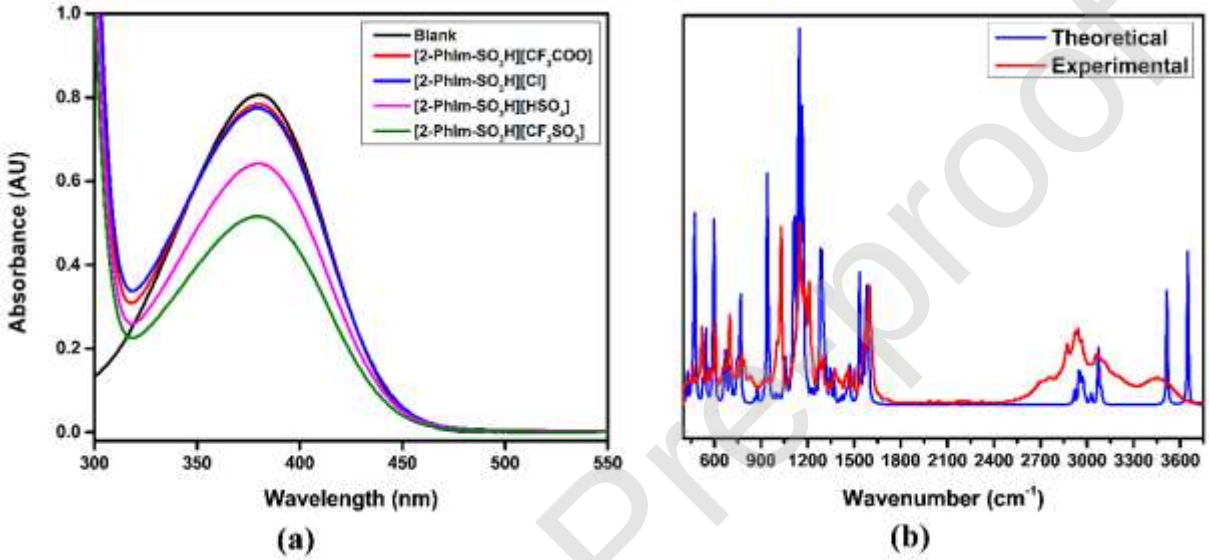

Fig. 2. (a) UV-Vis absorption spectra of 25 mM 4-nitroaniline in [2-PhIm-SO_3H][CF_3SO_3], [2-PhIm-SO_3H][HSO_4], [2-PhIm-SO_3H][Cl], and [2-PhIm-SO_3H][CF_3COO] IL catalysts. (b) Experimentally measured and theoretically calculated FT-IR spectra of the [2-PhIm-SO_3H][CF_3SO_3] IL catalyst.

3.1.2 Thermal stability characterization

The thermal stability of the synthesized IL [2-PhIm-SO_3H][CF_3SO_3] catalyst was studied using thermogravimetric analysis (TGA) under the nitrogen atmosphere and the results are shown in Fig. 3 (a). From the Fig. 3 (a), it can be seen that the synthesized catalyst shows high thermal stability up to 210 °C and the weight loss starts at and above 210 °C is evident from the change of the slope of TGA and shows complete degradation at above 425 °C. From the TGA study, it can be concluded that the catalysts have good thermal stability in the range of our reaction temperatures.

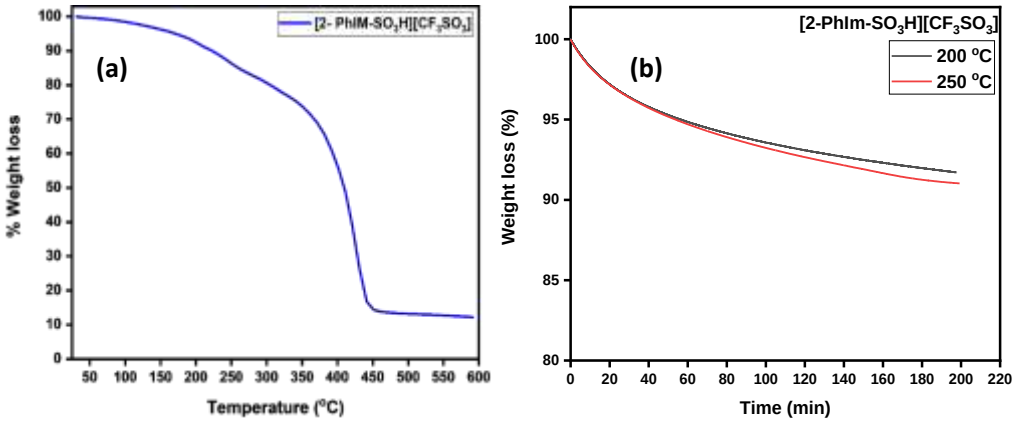

Fig. 3. (a) TGA analysis and (b) Isothermal TGA curves of the synthesized IL [2-PhIm-SO_3H][CF_3SO_3] catalyst.

The long term thermal stability of the synthesized IL catalyst [2-PhIm-SO_3H][CF_3SO_3] was also investigated by performing an isothermal TGA under nitrogen atmosphere for 3 h at 200°C and 250 °C temperature range. The nature of TGA curves for the IL catalyst [2-PhIm-SO_3H][CF_3SO_3] are depicted in the Fig. 3 (b) and it can be seen that slopes of the curves at both the temperatures (200°C and 250 °C) are almost constant up to 3 h, with 8% weight loss at 200°C, and 9% weight loss at 250 °C.

3.1.3 Elemental and mass analysis

The data of the electrospray ionization mass spectrometry (ESI-MS) for the IL [2-PhIm-SO_3H][CF_3SO_3] is given in the ESI (Fig. S8). The characterization evidence for the IL formation was provided by the analysis of ESI-MS in the positive ion mode and reported for the IL [2-PhIm-SO_3H][CF_3SO_3] (molecular formula $C_{14}H_{19}F_3N_2O_6S_2$) as follows: m/z calculated for $C_{14}H_{19}F_3N_2O_6S_2$ ($M+H^+$)=433.43, found at 282.8042 (positive ion mode) for the ionic liquid zwitterion molecular formula ($C_{13}H_{18}N_2O_3S$) m/z= 282.36 which is matched with the low resolution mass spectrometry (LRMS) value of the zwitterion. A sharp peak is observed at 418.7415 m/z. This peak is attributed to the decomposed zwitterion into 2-phenyl imidazoline and 1,4 butane sultone and 1,4-butanesultone association in gas phase with the zwitterion (zwitterion-1,4 butane sultone, m/z=282.10+136.02=418.12). Another peak appears at 146.8839 m/z corresponding to the 2-phenyl imidazoline (molecular formula $C_9H_{10}N_2$) which is formed in the decomposition of the zwitterion into 2-phenyl imidazoline.

The synthesized catalyst was dried under vacuum before its further use. The elemental analysis (C, H, N) was performed on a CHN elemental analyzer (PerkinElmer model 2400). Anal.

Calcd for [2-PhIm-SO_3H][CF_3SO_3] or ($C_{14}H_{19}F_3N_2O_6S_2$): C, 38.88; H, 4.43; N, 6.48 and found: %C = 38.95%, %H = 4.48% and %N = 6.42%. For IL [2-PhIm-SO_3H][HSO_4] or ($C_{13}H_{20}N_2O_7S_2$): C, 41.04; H, 5.30; N, 7.36 and found: %C = 41.14%, %H = 5.25%, and %N = 7.38%. For [2-PhIm-SO_3H][Cl] or ($C_{13}H_{19}ClN_2O_3S$): C, 48.97; H, 6.01; Cl, 11.12; N, 8.79 and found %C = 49.12%, %H = 6.11%, and %N = 8.72%. And for the IL [2-PhIm-SO_3H][CF_3COO] or ($C_{15}H_{19}F_3N_2O_5S$): C, 45.45; H, 4.83; F, 14.38; N, 7.07 and found: %C = 45.50%, %H = 4.85%, and %N = 7.03%

3.1.4 Hammett acidity values of the Brønsted acidic IL catalysts

The acidity of the Brønsted acidic IL catalysts was determined using UV-Vis spectroscopy. The values of the Hammett function for the IL catalysts were calculated using Eqn. 3 and reported in Table 1. From Table 1, it is evident that the Brønsted acidic IL catalyst [2-PhIm-SO_3H][CF_3SO_3] has lowest H_0 value (0.76), while IL [2-PhIm-SO_3H][CF_3COO] has the highest H_0 value (2.33). Lower H_0 value signifies the high acidic strength of the catalyst [75]. The overall acidity trend of the Brønsted acidic ILs was found in the following order: [2-PhIm-SO_3H][CF_3SO_3] > [2-PhIm-SO_3H][HSO_4] > [2-PhIm-SO_3H][Cl] > [2-PhIm-SO_3H][CF_3COO].

Table 1. The values of Hammett acidity function (H_0) for all Brønsted acidic IL catalysts.

ILs	A_{max}	[I](%)	[IH^+]%	H_o
None	1	100	0	-
[2-PhIm-SO_3H][CF_3SO_3]	0.52	64.09	35.90	0.76
[2-PhIm-SO_3H][HSO_4]	0.64	79.75	20.24	1.23
[2-PhIm-SO_3H][Cl]	0.77	96.14	03.85	2.17
[2-PhIm-SO_3H][CF_3COO]	0.78	97.26	02.73	2.33

3.2 Catalysts screening

The activity of [2-PhIm-SO_3H][CF_3SO_3], [2-PhIm-SO_3H][HSO_4], [2-PhIm-SO_3H][Cl], and [2-PhIm-SO_3H][CF_3COO] catalyst was tested under autogenous pressure at 150 °C for 5 h in biphasic reaction medium and the results are represented in Fig. 4. From Fig. 4, it can be seen that, that the Brønsted acidity of the IL catalyst has a large effect on 5-HMF product yield. It is reported that the nature of the anion of IL catalyst influences the acidity of which in-turn affects its catalytic activity [76]. Brønsted acidic IL catalyst [2-PhIm-SO_3H][CF_3SO_3] exhibits the highest 5-HMF yield (70%) after 5 h reaction time at 150 °C with an LA yield of 23%. In case of IL catalyst [2-PhIm-SO_3H][HSO_4], 65% yield of the 5-HMF was achieved with 19% LA yield at 150 °C and 5

h reaction time. Brønsted acidic IL catalyst [2-PhIm-SO_3H][Cl] and [2-PhIm-SO_3H][CF_3COO] gave 57% and 48% 5-HMF yield at 5 h and 150 °C, respectively. The LA yields were 16% and 10% using [2-PhIm-SO_3H][Cl] and [2-PhIm-SO_3H][CF_3COO] catalysts respectively. Among the tested Brønsted acidic IL catalysts, catalyst [2-PhIm-SO_3H][CF_3COO] exhibited a low (48%) 5-HMF yield, while, catalyst [2-PhIm-SO_3H][CF_3SO_3] showed better catalytic performance with 70% 5-HMF yield due to its high Brønsted acidity. The IL catalysts with $[HSO_4]^-$, $[Cl]^-$ and $[CF_3COO]^-$ anions showed remarkably low 5-HMF yield as compared to [2-PhIm-SO_3H][CF_3SO_3] catalyst because of their weak Brønsted acidity as obtained by Hammett acidity values in Table 1 and also theoretical DFT calculations (Table 3). The overall catalytic activity trends for the cellulose conversion into 5-HMF followed the order: [2-PhIm-SO_3H][CF_3SO_3] > [2-PhIm-SO_3H][HSO_4] > [2-PhIm-SO_3H][Cl] > [2-PhIm-SO_3H][CF_3COO].

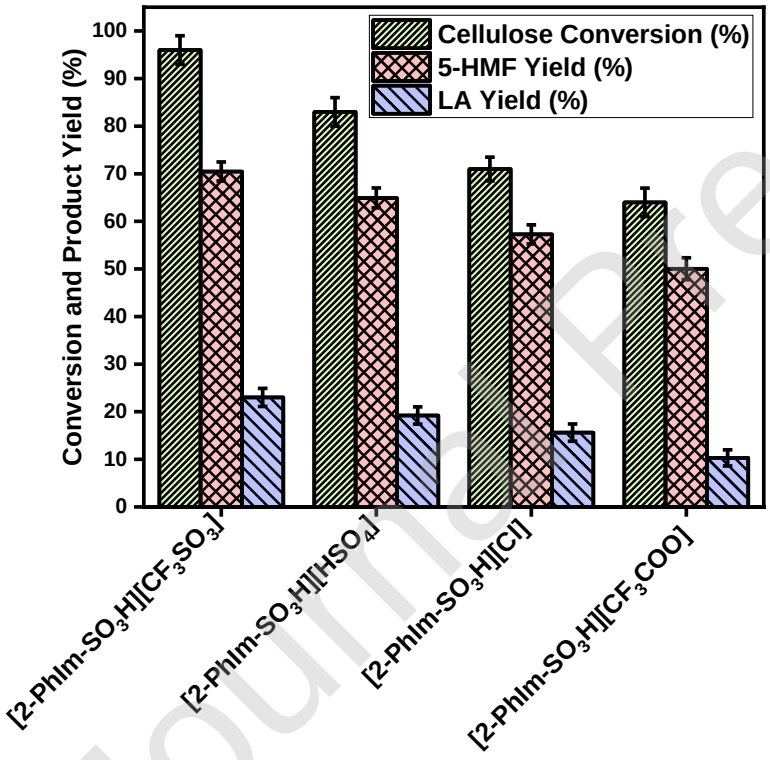

Fig. 4. Dependence of 5-HMF and LA yields on the four IL catalysts. Reaction conditions: 0.1 g cellulose; 0.3 g IL catalyst, Water: MIBK (1:10), t=5h, T= 150 °C, and 400 rpm.

3.3 Effect of temperature and time on the product yield

In order to obtain the maximum 5-HMF yield, the yield of the product was monitored as a function of time and temperature using Brønsted acidic IL [2-PhIm-SO_3H][CF_3SO_3] catalyst. MCC conversion was carried out in the temperature range of 110 °C -170 °C 5 h and the product analysis

results after 5h reaction time are shown in Fig. 5. From Fig. 5 it is clear that, as the reaction temperature increased from 110 °C to 150 °C, the yield of 5-HMF increased significantly and a maximum 70% yield of the 5-HMF was achieved at 150 °C and 5 h reaction time. When the reaction temperature was increased from 150 °C to 170 °C, the maximum 5-HMF yield decreased slightly to 55% due to rehydration reaction yielding more LA. At this temperature 34% yield of the LA was achieved which is slightly higher than 23% at 150 °C. It was also observed that formation of humin and other side products (LA and FA) become significant at 170 °C. Hence, the optimum reaction temperature for selective high 5-HMF yield is 150 °C.

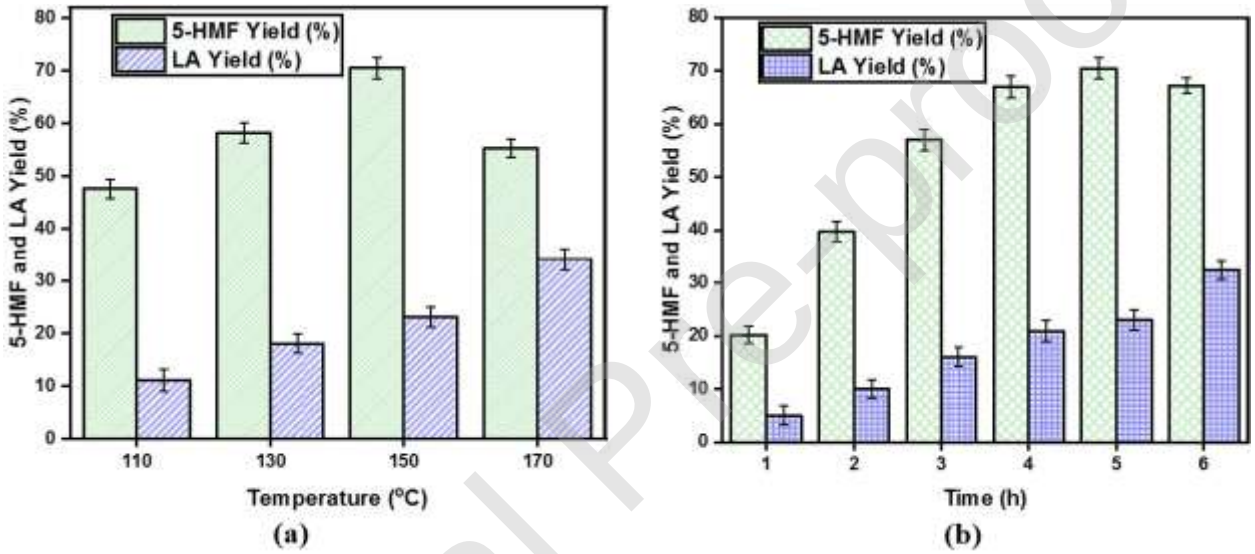

Fig. 5. Dependence of 5-HMF and LA yields on (a) reaction temperature with reaction condition: 0.1 g MCC; 0.3 g [2-PhIm-SO_3H][CF_3SO_3] IL catalyst, MIBK : water (10:1), 400 rpm, and (b) reaction time with reaction condition: 0.1 g MCC; 0.3 g [2-PhIm-SO_3H][CF_3SO_3] IL catalyst, MIBK: water (10:1), T= 150 °C, 400 rpm.

3.4 Effect of the solvent on the conversion of cellulose and 5-HMF yield

Different types of reaction media such as aqueous, organic, and biphasic (aqueous-organic) were investigated as solvents for the conversion of MCC and the results from this study are summarized in Table 2. In the presence of only aqueous medium (H_2O), only 47% yield of 5-HMF was achieved at 73% MCC conversion while the 5-HMF yield was very low (not more than 37%) at a low MCC conversion (49%) MIBK in only organic solvent. This low yield and low conversion of MCC is attributed to the robust and crystalline structure of MCC, which is less soluble in pure organic solvents. In case of only aqueous solvents, some amount of the black insoluble byproduct called

humin was observed. These results indicate that, humin formation becomes dominant in aqueous medium via inter or intramolecular polymerization of 5-HMF or glucose (due to the high reactivity of 5-HMF in a Brønsted acidic catalyst medium). In the biphasic solvent, MCC conversion and selective yield of the 5-HMF increases significantly since 5-HMF continuously gets extracted from the water to the organic phase (MIBK) due to the high partition coefficient of this phase modifier which suppresses the formation of undesired side products [77–79]. The effect of the amount of the water addition on 5-HMF yield was investigated and it was found that 1:10 volume ratio of water: MIBK gives a maximum of 70% 5-HMF yield at a 96% MCC conversion. In the biphasic system, the 5-HMF product gets extracted from the aqueous phase into the MIBK phase as soon as it is formed, preventing further conversion of 5-HMF into undesired side products. As the volume ratio of the water to MIBK is increased, the conversion of MCC as well as 5-HMF yield decreased due to the decreased accessibility of the acidic sites due to the dilution factor. On the other hand, increased concentration of water with MIBK limits the rate of the rehydration of the 5-HMF. Hence, an optimum ratio of MIBK to water (5:0.5) is needed to achieve high MCC conversion (96%) and high yield of the 5-HMF (70%).

Table 2. Effect of the organic and aqueous solvents on the cellulose conversion and 5-HMF yield.*

S. No.	Solvent (mL)	Cellulose Conversion (%)	HMF Yield (%)
1	H_2O (5.5)	73	47
2	MIBK (5.5)	49	37
3	MIBK (5.0)/ H_2O (0.5)	96	70
4	MIBK (4.5)/ H_2O (l.0)	90	63
5	MIBK (4.0)/ H_2O (l.5)	86	60
6	MIBK (3.5)/ H_2O (2.0)	81	52

*Reaction conditions: 0.1 g cellulose; 0.3 g IL catalyst, T= 150 °C, t=5h, and 400 rpm.

3.5 Effect of catalyst loading on 5-HMF yield

The effect of the catalyst [2-PhIm-SO_3H][CF_3SO_3] loading was varied in the range of 0.1-0.7 g to carried out the conversion of MCC at 150 °C for 5 h reaction time and shown in Fig. 6. When the amount of [2-PhIm-SO_3H][CF_3SO_3] catalyst was 0.1 g, the obtained 5-HMF yield was 38%. Further increase in the amount of catalyst to 0.3 g, increases 5-HMF to 70%. With increase in amount of catalyst loading beyond 0.3 g, the acidity of the reaction system is increased above

optimum and the 5-HMF yield falls due to the rehydration reaction giving LA, formic acid and polymerization byproducts of 5-HMF. At 0.7 g catalyst loading, the yield of 5-HMF become 36%. It is also reported in the earlier literature that the high Brønsted acidic reaction medium favors the LA formation. Hence, 0.3 g of IL was used in the reaction system for further investigations.

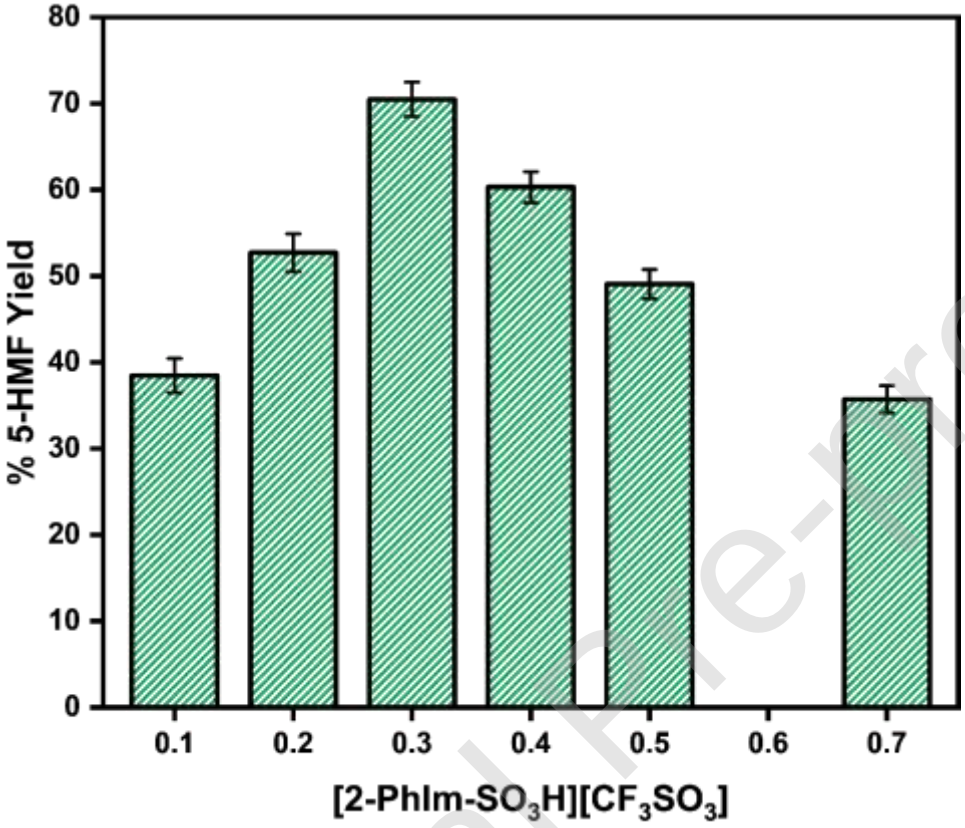

Fig. 6. Dependence of 5-HMF yield on the [2-PhIm-SO_3H][CF_3SO_3] catalyst loading. Reaction conditions: 0.1 g MCC; Water: MIBK (1:10), T= 150 °C, t= 5h, and 400 rpm.

3.6 Interaction and bond dissociation energies of the IL catalysts from DFT

The DFT optimized geometries of the individual anions ($[CF_3SO_3]^-$, $[HSO_4]^-$, $[CF_3COO]^-$), isolated cation ($[2\text{-PhIm-}SO_3H]^+$) and its zwitterionic form ([2-PhIm-SO_3]) are shown in Fig. S10 of ESI. The minimum energy configurations of [2-PhIm-SO_3H][CF_3SO_3], [2-PhIm-SO_3H][HSO_4], [2-PhIm-SO_3H][Cl], and [2-PhIm-SO_3H][CF_3COO] ion-pairs are shown in Fig. 7(a-d). The Brønsted acidity behavior of the IL catalysts were elucidated by considering the interaction and bond dissociation energies obtained from the energies of the optimized geometries using Eqns. 1 and 2. The tendency to donate the [H^+] ion with the formation of a conjugated base is called Brønsted acidity of the IL catalyst. The calculated interaction and O-H bond dissociation energies of the all the four ILs are given in Table 3. From the Table 3, it is evident that the interaction

energy between the cation and anion is maximum for [2-PhIm-SO_3H][Cl] and minimum for [2-PhIm-SO_3H][CF_3SO_3]. In [2-PhIm-SO_3H][Cl], the whole negative charge is localized over the chloride anion, whereas in case of the [2-PhIm-SO_3H][CF_3SO_3], [2-PhIm-SO_3H][HSO_4], and [2-PhIm-SO_3H][CF_3COO] ILs, the negative charge is spread over all the atoms of the anions. Moreover, as compared to the chloride anion, $[CF_3SO_3]^-$, $[HSO_4]^-$and $[CF_3COO]^-$ are large in size.

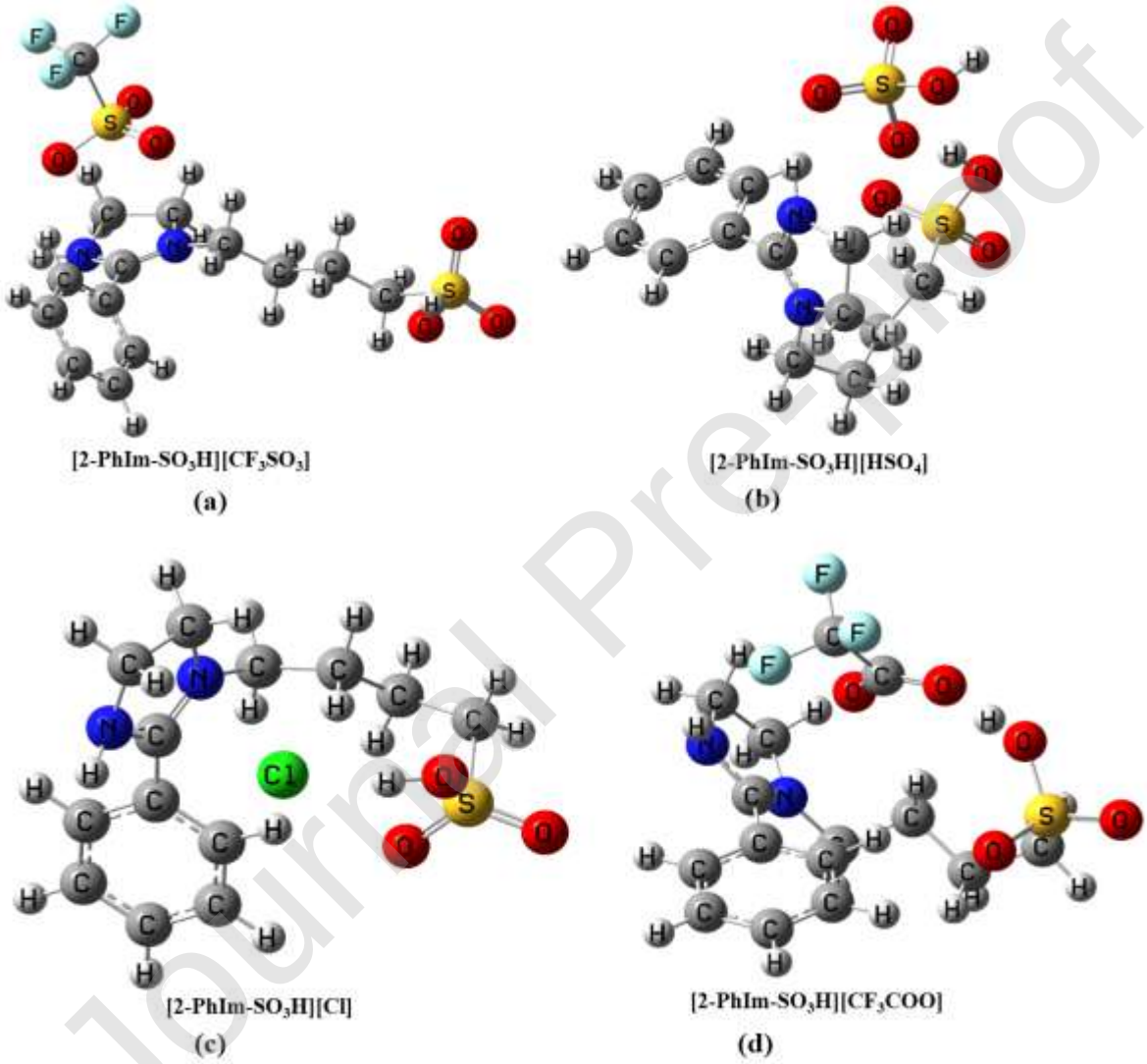

Fig. 7. Optimized structures of the ion-pairs of (a) [2-PhIm-SO_3H][CF_3SO_3], (b) [2-PhIm-SO_3H][HSO_4], (c) [2-PhIm-SO_3H][Cl], and (d) [2-PhIm-SO_3H][CF_3COO] ILs.

Hence, the maximum negative interaction energy of [2-PhIm-SO_3H][Cl] indicates its most stable and least reactive nature. On the other hand, [2-PhIm-SO_3H][CF_3SO_3] is least stable and highly

reactive in nature. The minimum stabilization of the IL catalyst [2-PhIm-SO_3H][CF_3SO_3] can also be explained by the O-H bond dissociation energies as given in Table 3. On the basis of the bond dissociation energies, the order of the stability of the ILs was found to be, [2-PhIm-SO_3H][CF_3COO] > [2-PhIm-SO_3H][Cl] > [2-PhIm-SO_3H][HSO_4] > [2-PhImSO_3H][CF_3SO_3]. Lower the bond dissociation energy, lower the stability of the IL and higher the acidity of the catalyst. Hence, the acidity trend of the catalysts can be placed in the following order: [2-PhIm-SO_3H][CF_3SO_3] > [2-PhIm-SO_3H][HSO_4] > [2-PhIm-SO_3H][Cl] > [2-PhIm-SO_3H][CF_3COO], which also corroborates well with the experimentally determined Hammett acidity order of the IL catalysts (Table 1).

In the optimized structures of the ion-pairs, we also observe that the orientation of the cationic tails depends on the anion type. The orientational preference of the anions around cationic moieties are depicted in the Fig. 8. The electrostatic potential surface (ESP) of the cation, anions and corresponding ion-pairs of the IL catalysts were obtained from the optimized geometries. In ESP structures shown in Fig. S11, the red color indicates the higher electron density region (high electrostatic potential reason) while the blue color indicates the lower electron density region (positive electrostatic potential). The green and yellow ESP surfaces represent neutral level. We observe that in the isolated form, all the anions' ESP surfaces are red in color and carrying the high negative charges (electron density). Also, in isolated form the cation ESP surface presented in blue color which indicates that the cations have low electron density and carrying low negative charge as compare to anion. In cation, oxygen atom represented in the red color indicates that they are holding some electron density. In the zwitterion form, the ESP surface shows maximum electron density on all the three oxygen atoms which are attached with the sulfur. After the combination with the protons, zwitterions makes the IL and generate a corresponding conjugate anion. The proton affinity of the zwitterion describes the ability of the molecules to combine with proton and get neutralized via generation of the conjugate anion. In IL catalyst as represented in Fig. S11, it is observed that all atoms on the 2-$PhIm^+$ ring, especially N atoms, carry most of the positive charge.

Table 3. Calculated interaction and bond dissociation energies of the Brønsted acidic IL catalysts.

IL	E_{int} **(kJ mol^{-1})**	E_{diss} **(kJ mol^{-1})**
[2-PhIm-SO_3H][CF_3SO_3]	-339.85	1297.23
[2-PhIm-SO_3H][HSO_4]	-369.10	1298.06

[2-PhIm-SO_3H][Cl]	-428.85		1317.84
[2-PhIm-SO_3H][CF_3COO]		-414.79	1326.92

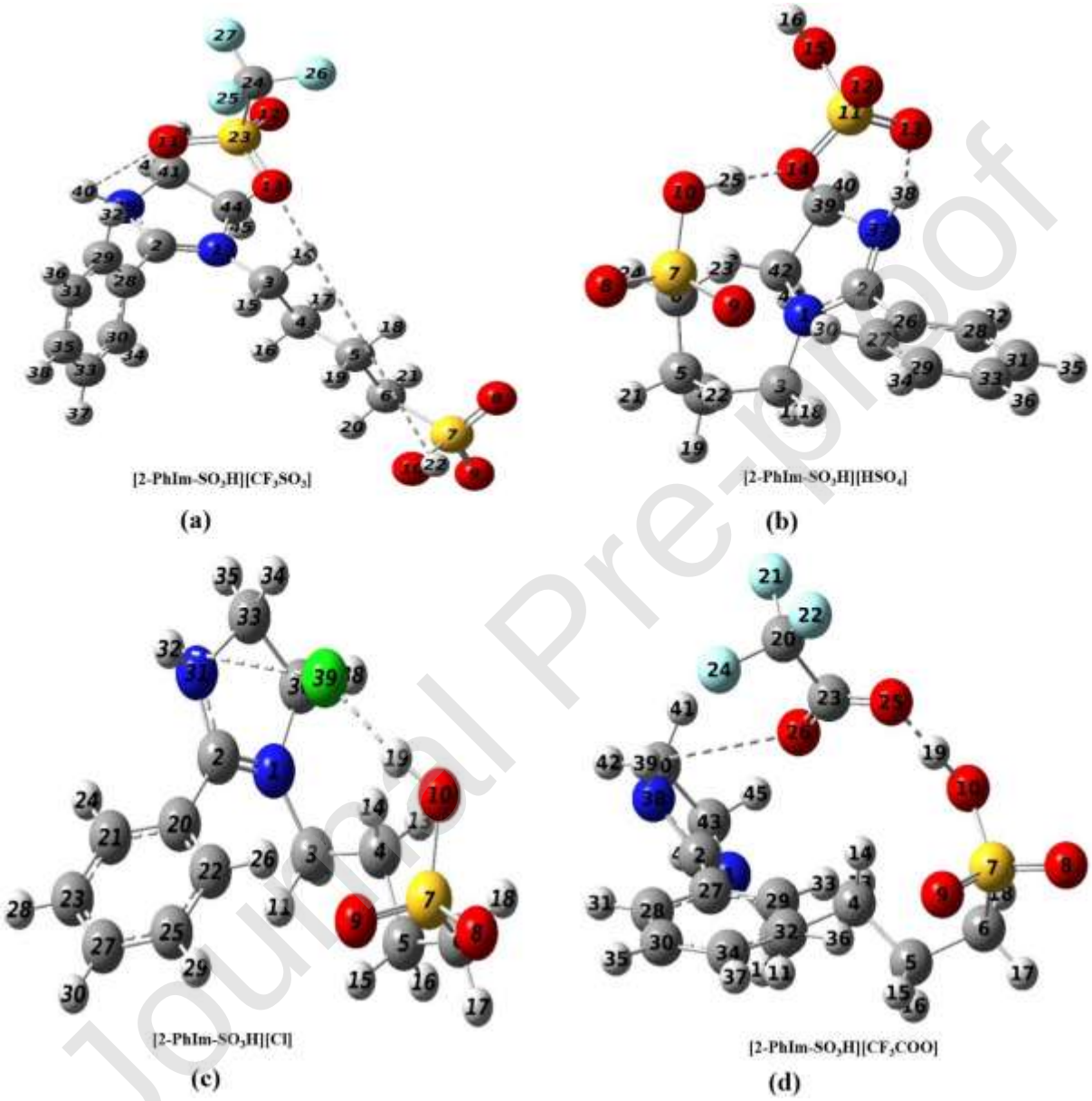

Fig. 8. Possible interactions (*dashed lines*) of the anions with acidic hydrogen associated with [2-PhIm-SO_3H]$^+$ cation in the ion-pairs of (a) [2-PhIm-SO_3H][CF_3SO_3], (b) [2-PhIm-SO_3H][HSO_4], (c) [2-PhIm-SO_3H][Cl], and (d) [2-PhIm-SO_3H][CF_3COO] ILs.

3.7 Frontier molecular orbital (FMO) analysis

The calculated HOMO and LUMO orbitals and their energies calculated from the optimized structures of the IL catalysts are represented in the Fig. 9. Similarly, the structures of the calculated HOMO and LUMO from the DFT optimized structure the individual cation and anions of the catalyst are represented in the ESI (Fig. S10). From Fig. 9, we observe that the HOMOs of all the four IL catalysts are distributed over 2-PhIm$^+$ ring of the cation. Whereas, the LUMOs are distributed over anions for [2-PhIm-SO_3H][CF_3SO_3], [2-PhIm-SO_3H][Cl], and [2-PhIm-SO_3H][CF_3COO] IL catalysts. For [2-PhIm-SO_3H][HSO_4] IL catalyst, the LUMO is localized on the phenyl ring, but away from the imidazolinium ring, as shown in Fig. 9.

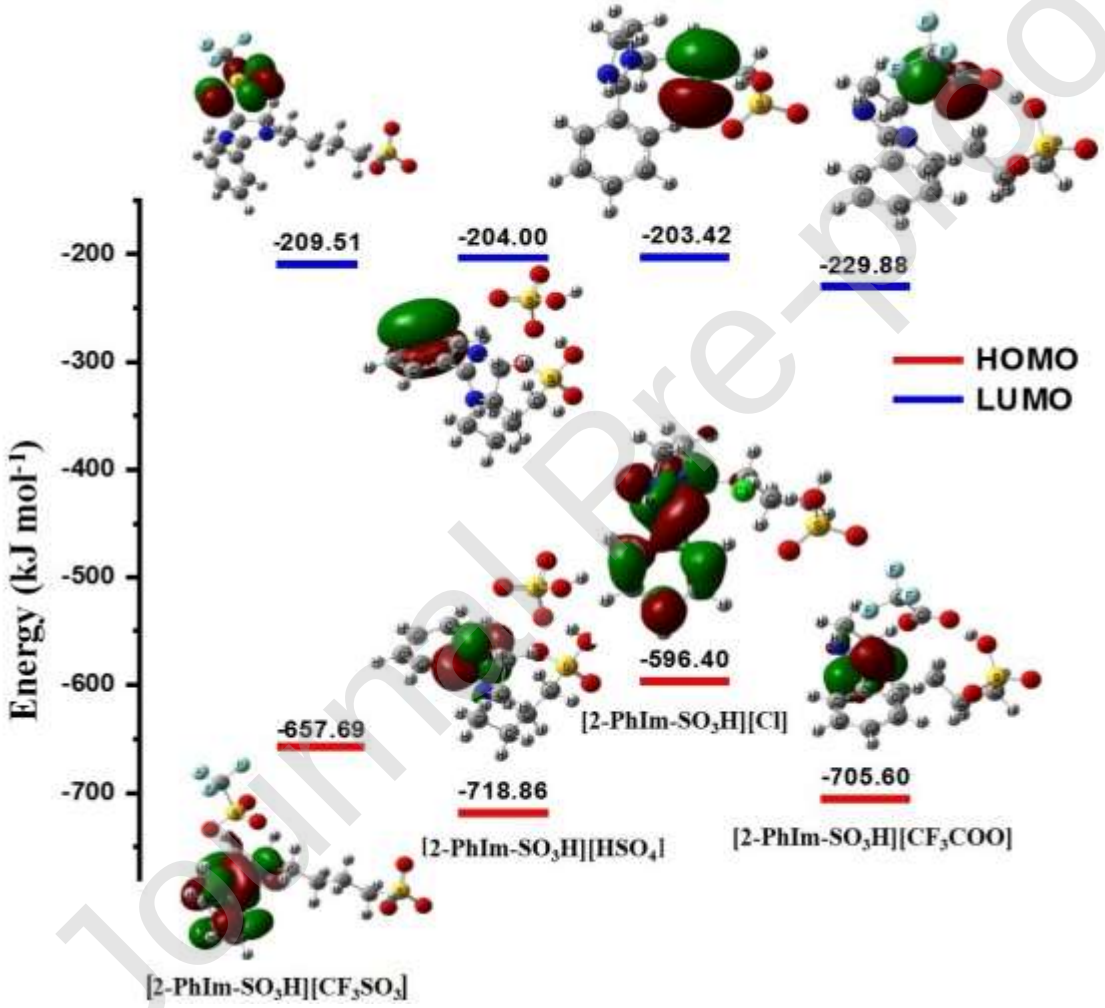

Fig. 9. Molecular highest occupied and lowest unoccupied orbital energy level diagram of the ion-pairs of IL catalysts. The HOMOs and LUMOs of the corresponding IL catalyst are also shown.

3.8 NBO and second order perturbation theory analyses of the Brønsted acidic IL catalysts

Using the DFT optimized structures of the IL catalysts, NBO analysis was carried out to obtain the population and extent of overlapping of the orbitals. The intramolecular orbital interactions in the IL ions and the intermolecular hyper-conjugative interactions in the ion-pairs of the ILs can be understood using the NBO analysis [80]. The interaction between the different species occurring due to the donation or acceptance of the electron(s) from the localized NBOs of the idealized Lewis structure to the vacant non-Lewis orbitals. This phenomenon is called electron delocalization corrections to the zeroth-order natural Lewis structures. In order to identify the donor-acceptor interactions within the IL ion-pairs, second-order perturbation energy correction in the stabilization energy, $E^{(2)}$, was calculated and the main donor-acceptor orbitals of the ions-pairs of the four ILs are reported in Fig. 10. On the basis of the second-order perturbation energy correction in stabilization energy, we selected the seven most strong donor-acceptor interactions between the molecular orbitals of the ion-pairs of each IL catalyst. Higher values of energy $E^{(2)}$ means strong interaction between the orbitals [81,82]. For each IL, the strongest donor-acceptor interaction between the molecular orbitals within the IL ion-pair and the value of $E^{(2)}$ are shown in Fig. 10. Other donor-acceptor orbitals having significant interactions are also represented in Fig. S12-S15 and given in Table S1 of the ESI.

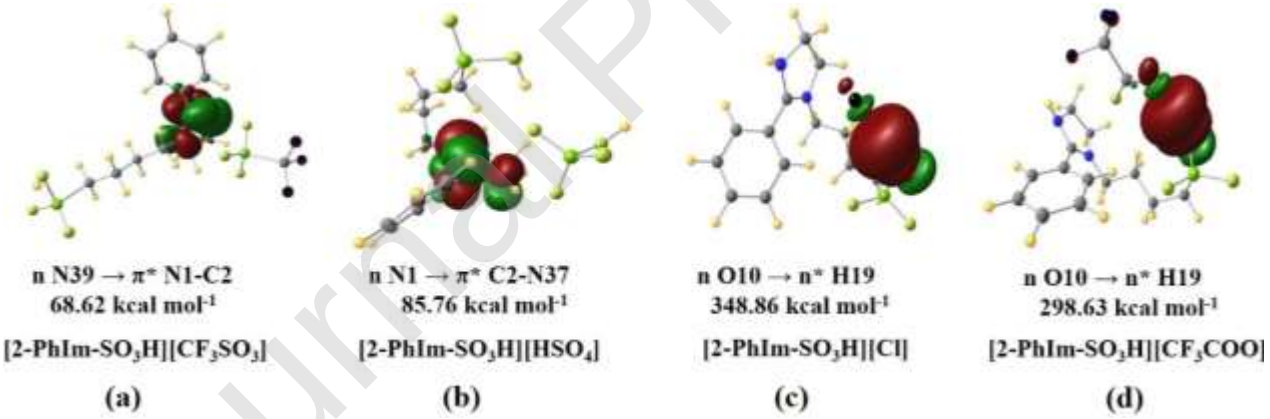

Fig. 10. Most energetic donor-acceptor hyper-conjugative interactions in the ion-pairs of (a) [2-PhIm-SO_3H][CF_3SO_3], (b) [2-PhIm-SO_3H][HSO_4], (c) [2-PhIm-SO_3H][Cl], and (d) [2-PhIm-SO_3H][CF_3COO] ILs.

As shown in the Fig. 10, IL catalyst [2-PhIm-SO_3H][CF_3SO_3] shows stronger interaction between non-bonding orbital of N39 → π^*N1-C2 with 68.62 kcal mol^{-1}. In case of IL catalyst [2-PhIm-SO_3H][HSO_4], strongest interaction between non-bonding orbital of N1 → π^*C2-N37 is seen with

85.76 kcal mol^{-1}. A strong interaction between non-bonding orbital of O10 → n^{*}H19 with the interaction energy of 348.86 kcal mol^{-1} is observed in IL catalyst [2-PhIm-SO_3H][Cl]. A similar interaction is observed between O10 → n^{*}H19 in case of [2-PhIm-SO_3H][CF_3COO] with 298.63 kcal mol^{-1}. It is interesting to note that, all the highest energy donor-acceptor transitions of the ILs is found within the cation orbitals only. As shown in Table S1 (and Fig. 10 and Fig. S12), in case of the catalyst [2-PhIm-SO_3H][CF_3SO_3], there is no donor-acceptor interaction between the orbitals of the anion (($[CF_3SO_3]^-$) and orbital of acidic hydrogen (H19). This results indicates that the acidic hydrogen in the O-H is free from the anion interaction in this IL catalyst. In case of the catalyst [2-PhIm-SO_3H][CF_3SO_3], the least or almost negligible interaction of the anion (($[CF_3SO_3]^-$) with the acidic hydrogen in O-H group is also confirmed with the low interaction energy formation as previously discussed through Table 3. Here, the presence of the minimum interaction between the anion and acidic hydrogen of cationic O-H group indicates that the cation and anion are loosely bonded to each other, leading to facile liberation of acidic proton of the IL catalyst. Similar observation is found for [2-PhIm-SO_3H][HSO_4] IL catalyst. In case of [2-PhIm-SO_3H][Cl] and [2-PhIm-SO_3H][CF_3COO], a transition of n Cl39 → n* H19 and n O25 → n* H19, respectively, shows that the acidic hydrogen has an interaction with the corresponding anion. From the Fig. 10 and Table 3, ILs [2-PhIm-SO_3H][CF_3SO_3] and [2-PhIm-SO_3H][HSO_4] do not show any interaction or transition between the acidic hydrogen and the anion. This shows that $[CF_3SO_3]^-$ and $[HSO_4]^-$ anions do not have any effect on the acidic proton of the -SO_3H group of the IL. Therefore, the proton is easily available, confirming the higher acidity of these two IL catalysts. In case of [2-PhIm-SO_3H][Cl] and [2-PhIm-SO_3H][CF_3COO], $[Cl]^-$and $[CF_3COO]^-$anions have appreciable interaction with acidic hydrogen and, therefore, causes the lower acidity of the catalyst. These results are in accordance with those observed through experimental Hammett acidity functions as well as with other DFT calculations discussed previously.

3.9 Comparison of results with reported literature

A comparison of the results of the present study already reported catalytic conversion of the cellulose to 5-HMF have been summarized in Table 4. The activity of the IL catalyst, [2-PhIm-SO_3H][CF_3SO_3], in this reaction was found be higher than most catalysts and comparable to all at their optimal process conditions. Z.D. Ding and co-workers reported 69% yield of the 5-HMF using [Emim][Ac] solvent and [C_4SO_3Hmim][CH_3SO_3] catalyst at 160 °C and 3.5 h reaction time. This study had to use high amount of the solvent and catalyst loading [83]. W. H. Hsu and

coworkers reported only 21% yield of 5-HMF from cellulose conversion [85]. Fang et al. could achieve 39% yield of the 5-HMF from cellulose conversion at 130 °C after a long reaction time (8 h) [84]. L. Zhou and co-workers reported 53% yield of the 5-HMF in a two-step reaction from cellulose conversion using bifunctional catalysts within 5 h reaction time and 120 °C [85]. Chou's group reported the conversion of cellulose into 5-HMF using catalytic amounts of $FeCl_2$ in ILs. Their study reported 34% yield of the 5-HMF under the optimized conditions [86]. Binder and co-workers reported 54% yield of the 5-HMF from cellulose conversion in the presence of ILs and metal chlorides as co-catalyst at 140 °C and 2 h reaction time. Binder and co-workers used metal chlorides ($CrCl_2$) with mineral acids as their catalyst system and a mixture of N,N-dimethylacetamide (DMAc) containing lithium chloride (LiCl), DMAc-LiCl and [EMIM]Cl as solvent and additive. In our study higher MCC conversion and product yields were obtained using single, benign, noncorrosive, IL catalyst in one step at low temperature and time.

Table 4. Summary of the results of cellulose conversion to 5-HMF from literature compared with present study.

Substrate	**Catalyst**	**Solvent**	**Time (h)**	**Temperature (°C)**	**Yield of 5-HMF (%)**	**Ref.**
Cellulose	$[C_4SO_3Hmim][CH_3SO_3]$ (1.5 mL) with $CuCl_2$	[Emim][Ac] (10 mL) + H_2O (0.2 mL)	3.5	160	69	[83]
Cellulose	[EMIM][Cl] (0.17 g)	H_2O/Cellulose= 10	3	120	21	[87]

Cellulose	$[Hnmp]Zn_2Cl_5$	[BMIM][Cl] (10 g) + DMSO (60 g)	8	130	39	[84]
Cellulose	$Cr([PSMIM]HSO_4])_3$	[BMIM][Cl] (2 g) + DMSO (60 g)	5	120	53	[85]
Cellulose	1-(4-sulfonic acid) butyl-3-methylimida-zolium hydrogen sulfate + $FeCl_2$	MIBK (8 mL), P=1 bar	5	150	34	[86]
Cellulose	$CrCl_2$ (25 mol%) + HCl (5 mol%)	DMA + LiCl (10%) + [EMIM][Cl] (60 wt%)	2	140	54	[88]
Cellulose	$[2\text{-}PhIm\text{-}SO_3H][CF_3SO_3]$	MIBK (5 mL) + H_2O (0.5 mL)	5	150	70	This study

3.10 Recyclability of the catalysts

Finally, the recyclability of the IL catalyst was studied for the cellulose conversion at 150 °C and 5 h reaction time. At the end of the reaction, the insolubles which include residual MCC and humin were first removed by centrifugation, followed by extraction of 5-HMF from the aqueous phase with ethyl acetate. Finally, the resultant aqueous phase contains IL which was heated in a vacuum

drier to remove residual ethyl acetate. Further, the recycled catalyst was reused following the addition of fresh cellulose and MIBK for the following consecutive cycles. The recyclability results for one of the IL catalysts [2-PhIm-SO_3H][CF_3SO_3] are presented in Fig. 11. It is clear from the figure that the recyclability of this catalyst is indeed encouraging as there is slight decline in the yield of 5-HMF from 70% in the fresh run to 63% at the end of the fourth cycle. The observation of this small decline in the yield is attributed to the slight weight loss of the catalyst during the extraction procedure. The incomplete extraction of the byproducts formed during the cellulose conversion in ethyl acetate at lab scale shows this slight decrease which can be overcome during scale-up of the process in a well-designed extraction equipment.

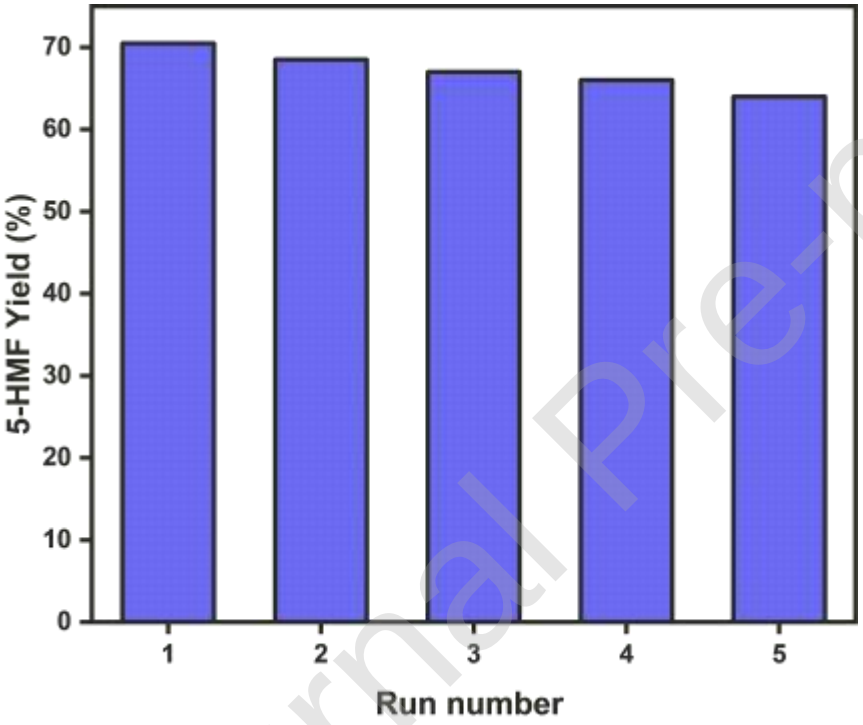

Fig. 11. Recyclability of the Brønsted acidic IL catalyst [2-PhIm-SO_3H][CF_3SO_3]. Reaction conditions: 0.1 g MCC; Water: MIBK (1:10), T= 150 °C, t= 5h, and 400 rpm.

4. Conclusions

A series of the Brønsted acidic IL catalysts were synthesized by varying the anions and tested in the one-step conversion of MCC into 5-HMF and LA in a biphasic solvent system. These laboratory synthesized Brønsted acidic IL catalysts were characterized using ^{1}H, ^{13}C NMR, FT-IR, TGA, and UV-Vis spectroscopy and supplemented with theoretical calculations. A highest yield of 70% 5-HMF with 23% yield of LA was achieved from MCC conversion using [2-PhIm-SO_3H][CF_3SO_3] catalyst at 150 °C and 5 h reaction time with a MIBK to water ratio of 5:0.5. The

catalytic activity trend of the Brønsted acid IL catalysts follows the order: [2-PhIm-SO_3H][CF_3SO_3] > [2-PhIm-SO_3H][HSO_4] > [2-PhIm-SO_3H][Cl] > [2-PhIm-SO_3H][CF_3COO] which is similar to the acidity trends of the ILs. A remarkable correlation was established between the experimentally obtained Brønsted acidity of the ILs catalyst and DFT calculations. The calculated high HOMO energy was dominant on the anion while low LUMO energy was dominant on the cation of the IL catalyst. From the DFT optimized structures of the IL catalysts, ESPs were generated which clearly show the distribution of the electron density over the whole IL, cation and corresponding anions. The calculated main second order perturbation stabilization energy interactions between the donor-acceptor in the Brønsted acidic ILs revealed the most stable and high energy interactions of the IL catalyst [2-PhIm-SO_3H][CF_3SO_3], [2-PhIm-SO_3H][HSO_4], [2-PhIm-SO_3H][Cl], and [2-PhIm-SO_3H][CF_3COO. From the second order perturbation analysis, cation-anion interaction indicated that the weakest interaction of the anion with acidic hydrogen is ascribed to the [2-PhIm-SO_3H][CF_3SO_3] and [2-PhIm-SO_3H][HSO_4] catalysts, while the strongest interaction of the anion with acidic hydrogen is ascribed to the [2-PhIm-SO_3H][Cl] and [2-PhIm-SO_3H][CF_3COO] IL catalysts. The activities of these IL catalysts in the MCC conversion to 5-HMF and LA reaction were observed to be well and correlated with their structures. This structure-activity relationships have helped us in developing a promising environmentally benign catalyst and reaction system for MCC conversion into the important 5-HMF and LA platform chemicals.

Credit Authors Statement

Komal Kumar, Conceptualization, Methodology, synthesis of catalyst, and performed the experiments, data analysis, and prepared the original manuscript. Vikas Khatri, Conceptualization, data analysis write, and edit the manuscript. Sreedevi Upadhyayula, write and reviewed, edited the manuscript, and supervised the research. Hemant K. Kashyap write, Editing, revision, and guidance. All authors have read and agreed to the published version of the manuscript.

Declaration of interest

There are no conflicts to declare.

References

[1] M. Olkiewicz, N. V. Plechkova, M.J. Earle, A. Fabregat, F. Stüber, A. Fortuny, J. Font, C. Bengoa, Appl. Catal. B Environ. 181 (2016) 738–746.

[2] N. Shi, Q. Liu, T. Wang, L. Ma, Q. Zhang, Green Chem. 15(7) (2013) 1967–1974.

[3] X. Li, Q. Xia, V.C. Nguyen, K. Peng, X. Liu, N. Essayem, Y. Wang, Catal. Sci. Technol. 6 (2016) 7586–7596.

[4] A. Deneyer, E. Peeters, T. Renders, S. Van den Bosch, N. Van Oeckel, T. Ennaert, T. Szarvas, T.I. Korányi, M. Dusselier, B.F. Sels, Nat. Energy 3 (2018) 969–977.

[5] M. Stöcker, Angew. Chemie - Int. Ed. 47 (2008) 9200–9211.

[6] R.J. Van Putten, J.C. Van Der Waal, E. De Jong, C.B. Rasrendra, H.J. Heeres, J.G. De Vries, Chem. Rev. 113 (2013) 1499–1597.

[7] P. Anbarasan, Z.C. Baer, S. Sreekumar, E. Gross, J.B. Binder, H.W. Blanch, D.S. Clark, F. Dean Toste, Nature 491 (2012) 235–239.

[8] K. Wang, J. Jiang, X. Liang, H. Wu, J. Xu, ACS Sustain. Chem. Eng. 6 (2018) 15092–15099.

[9] V. Choudhary, S.I. Sandler, D.G. Vlachos, ACS Catal. 2 (2012) 2022–2028.

[10] L. Liu, Z. Li, W. Hou, H. Shen, Carbohydr. Polym. 181 (2018) 778–784.

[11] Y.Z. Qin, M.H. Zong, W.Y. Lou, N. Li, ACS Sustain. Chem. Eng. 4 (2016) 4050–4054.

[12] E. Nikolla, Y. Román-leshkov, M. Moliner, M.E. Davis, Acs Catal. (2011) 1–8.

[13] K. Kumar, F. Parveen, T. Patra, S. Upadhyayula, New J. Chem. 42 (2018) 228–236.

[14] L. Zhou, R. Liang, Z. Ma, T. Wu, Y. Wu, Bioresour. Technol. 129 (2013) 450–455.

[15] G.D. Yadav, A.R. Yadav, Chem. Eng. J. 243 (2014) 556–563.

[16] K. Kumar, A. Dahiya, T. Patra, S. Upadhyayula, ChemistrySelect 3 (2018) 6242–6248.

[17] T. Boonyakarn, P. Wataniyakul, P. Boonnoun, A.T. Quitain, T. Kida, M. Sasaki, N. Laosiripojana, B. Jongsomjit, A. Shotipruk, Ind. Eng. Chem. Res. 58 (2019) 2697–2703.

[18] G. Portillo Perez, M.J. Dumont, Chem. Eng. J. 382 (2020).

[19] A. Mukherjee, M.J. Dumont, V. Raghavan, Biomass and Bioenergy 72 (2015) 143–183.

[20] R.S. Thombal, V.H. Jadhav, Appl. Catal. A Gen. 499 (2015) 213–216.

[21] X. Qi, M. Watanabe, T.M. Aida, R.L. Smith, Green Chem. 11 (2009) 1327–1331.

[22] S. Eminov, J.D.E.T. Wilton-Ely, J.P. Hallett, ACS Sustain. Chem. Eng. 2 (2014) 978–981.

[23] L.T. Mika, E. Cséfalvay, Á. Németh, Chem. Rev. 118 (2018) 505–613.

[24] F. Lai, F. Yan, P. Wang, S. Wang, S. Li, Z. Zhang, Chem. Eng. J. 396 (2020).

[25] A. Rahimi, A. Ulbrich, J.J. Coon, S.S. Stahl, Nature 515 (2014) 249–252.

[26] E.M. Rubin, Nature 454 (2008) 841–845.

[27] Suhas, V.K. Gupta, P.J.M. Carrott, R. Singh, M. Chaudhary, S. Kushwaha, Bioresour. Technol. 216 (2016) 1066–1076.

[28] M. Jarvis, Nature 426 (2003) 611–612.

[29] X. Li, K. Peng, Q. Xia, X. Liu, Y. Wang, Chem. Eng. J. 332 (2018) 528–536.

[30] H. Xia, S. Xu, X. Yan, S. Zuo, Fuel Process. Technol. 152 (2016) 140–146.

[31] O. Akpinar, K. Erdogan, S. Bostanci, Carbohydr. Res. 344 (2009) 660–666.

[32] A.A. Rosatella, S.P. Simeonov, R.F.M. Frade, C.A.M. Afonso, Green Chem. 13 (2011) 754–793.

[33] M. Hara, Energy Environ. Sci. 3 (2010) 601–607.

[34] R.R. Singhania, A.K. Patel, R.K. Sukumaran, C. Larroche, A. Pandey, Bioresour. Technol. 127 (2013) 500–507.

[35] Y. Zhao, W.-J. Lu, H.-T. Wang, Chem. Eng. J. 150 (2009) 411–417.

[36] Z.-D. Ding, J.-C. Shi, J.-J. Xiao, W.-X. Gu, C.-G. Zheng, H.-J. Wang, Carbohydr. Polym. 90 (2012) 792–798.

[37] L. Zhou, Y. He, Z. Ma, R. Liang, T. Wu, Y. Wu, Carbohydr. Polym. 117 (2015) 694–700.

[38] S.S. Chen, I.K.M. Yu, D.C.W. Tsang, A.C.K. Yip, E. Khan, L. Wang, Y.S. Ok, C.S. Poon, Chem. Eng. J. 327 (2017) 328–335.

[39] J.P. Hallett, T. Welton, (2011) 3508–3576.

[40] P. Wasserscheid, W. Keim, Angew. Chemie 39 (2000) 3772–3789.

[41] K. Kumar, V. Khatri, F. Parveen, H.K. Kashyap, S. Upadhyayula, Sustain. Energy Fuels (2020).

[42] A. Stark, Energy Environ. Sci. 4 (2011) 19–32.

[43] C. Fehér, S. Tomasek, J. Hancsók, R. Skoda-Földes, Appl. Catal. B Environ. 239 (2018) 52–60.

[44] R.P. Swatloski, S.K. Spear, J.D. Holbrey, R.D. Rogers, J. Am. Chem. Soc. 124 (2002) 4974–4975.

[45] H. Zhang, J. Wu, J. Zhang, J. He, Macromolecules 38 (2005) 8272–8277.

[46] T. Heinze, K. Schwikal, S. Barthel, Macromol. Biosci. 5 (2005) 520–525.

[47] A. Parviainen, A.W.T. King, I. Mutikainen, M. Hummel, C. Selg, L.K.J. Hauru, H. Sixta, I. Kilpeläinen, ChemSusChem 6 (2013) 2161–2169.

[48] Y. Liu, W. Xiao, S. Xia, P. Ma, Carbohydr. Polym. 92 (2013) 218–222.

[49] P. Zhang, Z. Jiang, Y. Cui, G. Xie, Y. Jin, L. Guo, Y. Xu, Q. Zhang, X. Li, Appl. Catal. B Environ. 255 (2019) 117757.

[50] B.S. Caldas, C.S. Nunes, P.R. Souza, F.A. Rosa, J. V. Visentainer, O. de O.S. Júnior, E.C. Muniz, Appl. Catal. B Environ. 181 (2016) 289–297.

[51] J.P. Hallett, T. Welton, Chem. Rev. 111 (2011) 3508–3576.

[52] Z. Zhang, Z.K. Zhao, Bioresour. Technol. 101 (2010) 1111–4.

[53] Y. Su, H.M. Brown, G. Li, X.D. Zhou, J.E. Amonette, J.L. Fulton, D.M. Camaioni, Z.C. Zhang, Appl. Catal. A Gen. 391 (2011) 436–442.

[54] S. Xiao, B. Liu, Y. Wang, Z. Fang, Z. Zhang, Bioresour. Technol. 151 (2014) 361–366.

[55] B.F.M. Kuster, Carbohydr. Res. 54 (1977) 177–183.

[56] Y. Román-Leshkov, J.A. Dumesic, Top. Catal. 52 (2009) 297–303.

[57] N. Shi, Q. Liu, T. Wang, L. Ma, Q. Zhang, Green Chem. 15 (2013) 1967–1974.

[58] P. Bhaumik, P.L. Dhepe, RSC Adv. 3 (2013) 17156–17165.

[59] T.S. Hansen, J. Mielby, A. Riisager, Green Chem. 13 (2011) 109–114.

[60] H. Li, Q. Zhang, X. Liu, F. Chang, Y. Zhang, W. Xue, S. Yang, Bioresour. Technol. 144 (2013) 21–27.

[61] K. Zhuo, Q. Du, G. Bai, C. Wang, Y. Chen, J. Wang, Carbohydr. Polym. 115 (2015) 49–53.

[62] C. Lee, W. Yang, R.G. Parr, Phys. Rev. B 37 (1988) 785–789.

[63] A.D. Becke, J. Chem. Phys. 96 (1992) 2155–2160.

[64] M.J. Frisch, J.A. Pople, J.S. Binkley, J. Chem. Phys. 80 (1984) 3265–3269.

[65] J.R.C. M.J. Frisch, G.W. Trucks, H.B. Schlegel, G.E. Scuseria, M.A. Robb, S.S.I. J.A. Montgomery, Jr., T. Vreven, K.N. Kudin, J.C. Burant, J.M. Millam, G.A.P. J. Tomasi, V. Barone, B. Mennucci, M. Cossi, G. Scalmani, N. Rega, T. H. Nakatsuji, M. Hada, M. Ehara, K. Toyota, R. Fukuda, J. Hasegawa, M. Ishida, H.P.H. Nakajima, Y. Honda, O. Kitao, H. Nakai, M. Klene, X. Li, J.E. Knox, A.J. J.B. Cross, C. Adamo, J. Jaramillo, R. Gomperts, R.E. Stratmann, O. Yazyev, G.A. Austin, R. Cammi, C. Pomelli, J.W. Ochterski, P.Y. Ayala, K. Morokuma, A.D.D. Voth, P. Salvador, J.J. Dannenberg, V.G. Zakrzewski, S.

Dapprich, J.B.F. M.C. Strain, O. Farkas, D.K. Malick, A.D. Rabuck, K. Raghavachari, A. J.V. Ortiz, Q. Cui, A.G. Baboul, S. Clifford, J. Cioslowski, B.B. Stefanov, G. Liu, M.A.A.-L. Liashenko, P. Piskorz, I. Komaromi, R.L. Martin, D.J. Fox, T. Keith, W.C. C.Y. Peng, A. Nanayakkara, M. Challacombe, P.M.W. Gill, B. Johnson, J.A.P. M.W. Wong, C. Gonzalez, Inc., Wallingford CT, (2004).

[66] E.D. Glendening, A.E. Reed, J.E. Carpenter, F. Weinhold, QCPE Bull. (1990).

[67] P.A. Hunt, B. Kirchner, T. Welton, Chem. - A Eur. J. 12 (2006) 6762–6775.

[68] A.E. REED, L.A. CURTISS, F. WEINHOLD, Chem. Rev. (1988) 899–926.

[69] C. Thomazeau, H. Olivier-Bourbigou, L. Magna, S. Luts, B. Gilbert, J. Am. Chem. Soc. 125 (2003) 5264–5265.

[70] K. Kondamudi, P. Elavarasan, P.J. Dyson, S. Upadhyayula, J. Mol. Catal. A Chem. 321 (2010) 34–41.

[71] F. Tao, H. Song, L. Chou, Bioresour. Technol. 102 (2011) 9000–9006.

[72] A.P. Scott, L. Radom, J. Phys. Chem. 100 (1996) 16502–16513.

[73] D. Xing, B. Lu, H. Wang, J. Zhao, Q. Cai, New J. Chem. 41 (2016) 387–392.

[74] L. Zhang, G. Xi, J. Zhang, H. Yu, X. Wang, Bioresour. Technol. 224 (2017) 656–661.

[75] R. Kore, R. Srivastava, Tetrahedron Lett. 53 (2012) 3245–3249.

[76] F. Tao, H. Song, L. Chou, Bioresour. Technol. 102 (2011) 9000–9006.

[77] J.N. Chheda, J. a Dumesic, Science (80-.). 312 (2006) 1933–1937.

[78] B. Saha, M.M. Abu-Omar, Green Chem. 16 (2014) 24–38.

[79] L.C. Blumenthal, C.M. Jens, J. Ulbrich, F. Schwering, V. Langrehr, T. Turek, U. Kunz, K. Leonhard, R. Palkovits, ACS Sustain. Chem. Eng. 4 (2016) 228–235.

[80] N. Choudhary, S. Bee, A. Gupta, P. Tandon, Comput. Theor. Chem. 1016 (2013) 8–21.

[81] I. Tankov, R. Yankova, J. Mol. Liq. 277 (2019) 241–253.

[82] H. Safia, L. Ismahan, G. Abdelkrim, C. Mouna, N. Leila, M. Fatiha, J. Mol. Liq. 280 (2019) 218–229.

[83] Z.D. Ding, J.C. Shi, J.J. Xiao, W.X. Gu, C.G. Zheng, H.J. Wang, Carbohydr. Polym. 90 (2012) 792–798.

[84] J. Fang, W. Zheng, K. Liu, H. Li, C. Li, Chem. Eng. J. 385 (2020).

[85] L. Zhou, R. Liang, Z. Ma, T. Wu, Y. Wu, Bioresour. Technol. 129 (2013) 450–455.

[86] F. Tao, H. Song, L. Chou, ChemSusChem 3 (2010) 1298–1303.

[87] W.H. Hsu, Y.Y. Lee, W.H. Peng, K.C.W. Wu, Catal. Today 174 (2011) 65–69.

[88] J.B. Binder, R.T. Raines, J. Am. Chem. Soc. 131 (2009) 1979–1985.